



Elastic properties and frequency characteristics of a piezo-active 3–0-type corundum-containing composite

P. A. Borzov¹ · S. E. Filippov¹ · V. Yu. Topolov² · O. E. Brill¹ · A. E. Panich¹

Received: 15 February 2018 / Accepted: 2 May 2018 / Published online: 23 May 2018
© Springer International Publishing AG, part of Springer Nature 2018

Abstract

A 3–0-type composite, that contains the PZT-type ferroelectric and corundum ceramics, is characterised as a piezoelectric material with relatively stable resonance frequencies for the planar and thickness modes of oscillation. The 3–0-type composite is manufactured by solid state sintering, the resulting composite microgeometry is studied by electronic microscopy, and parameters of the composite are measured by using the resonance-antiresonance method. It is observed that almost equal volume fractions of corundum m_c and air pores m_p are detected in the composite samples at $0.05 < m_c < 0.18$. The presence of both the corundum inclusions and air pores at an almost equal volume fraction influences the elastic properties and resonance frequencies. Experimental results on the elastic properties and frequency characteristics of the composite are interpreted in terms of a model that takes into account the electromechanical interaction between the 3–0 ferroelectric ceramic/corundum and 3–0 ferroelectric ceramic/pore regions. Effective electromechanical properties and related parameters of the composite are evaluated in terms of the effective field method and dilute approximation. The studied 3–0-type composite has potential to be applied as an active element of piezoelectric transducers, sensors, and other piezotechnical devices.

Keywords 3–0-type composite · Ferroelectric ceramic · Corundum ceramic · Elastic properties · Resonance and antiresonance frequencies · Composite model

1 Introduction

In recent decades, considerable effort has been made to manufacture novel and highly effective composites and predict their properties and related parameters for specific applications. The group of piezo-active composites is vast due to the large number of components that are involved for the design of such composites and the potential to improve and tailor their piezoelectric performance. These components are often chosen among ferroelectric ceramics (FCs), ferroelectric single crystals, and polymers [1–3], and each group of these materials can actively influence the piezoelectric properties of the composites. Piezo-active composites based on FCs are of

interest due to their effective electromechanical properties and related parameters [1–3] which are to be taken into account in piezotechnical applications [4] such as piezoelectric sensors, transducers, hydrophones, and energy-harvesting, medical ultrasonic, and non-destructive testing devices. The effective properties and parameters of the composite based on FC depend on the properties of components, microgeometry, technological factors, and poling conditions. By appropriate design of the piezoelectric composite, one can vary an anisotropy of the piezoelectric, elastic, and dielectric properties and electromechanical coupling factors [4]. Undoubtedly, an improvement of some parameters of the composite in comparison to the similar parameters of its FC component facilitates applications of the composite material.

Among the modern two-component piezo-active composites with α – β connectivity (written in terms of Ref. [5], where $\alpha = 0, 1, 2$, or 3, and $\beta = 0, 1, 2$, or 3), the 3– β composites [2] have been studied to a lesser degree in comparison to the widespread 2–2, 1–3, and 0–3 FC/polymer composites [1, 4]. A piezoelectric performance of the 3– β FC/polymer composites studied in work [2] suggests that these materials can be competitive because of their hydrostatic piezoelectric

✉ V. Yu. Topolov
vutopolov@sfedu.ru

¹ Institute of High Technologies and Piezotechnics, Southern Federal University, 10 Milchakov Street, Rostov-on-Don, Russia 344090

² Department of Physics, Southern Federal University, 5 Zorge Street, Rostov-on-Don, Russia 344090

parameters, piezoelectric sensitivity and anisotropy. In recent decades, various inorganic components such as clay, sand, and cement components have been used [6–10] to improve some effective parameters of the FC-based composites. Examples of the effective piezoelectric and dielectric properties of a ceramic composite that comprises α -Al₂O₃ (corundum) and the PKR-1 FC based on Pb(Zr, Ti)O₃ are shown in experimental work [10]. Among the studied effective parameters, we mention piezoelectric coefficients d_{3j}^* , dielectric permittivity $\epsilon_{33}^{*\sigma}$ of the stress-free sample, and sound velocities at longitudinal and thickness oscillation modes, and these parameters are represented as functions of the volume fraction of α -Al₂O₃ in the range from 0 to 0.6 [10]. Micrographs of the composite from work [10] are related to the volume fractions of α -Al₂O₃ 0.10, 0.18, 0.33, 0.46, and 0.57. Of an independent interest is a non-monotonic volume-fraction dependence of the piezoelectric coefficient d_{33}^* for volume fractions of α -Al₂O₃ under 0.20; however, the experimental d_{33}^* curve in this volume-fraction range is based on three points only and clearly more data in this area is necessary [10]. In general, the piezoelectric properties, electromechanical coupling, and related parameters of the PZT-type FC/ α -Al₂O₃ composite were also not considered [10] in detail for small volume fractions of α -Al₂O₃.

The corundum component is characterised by Young’s modulus that is larger than the elastic moduli of the FC component, and the dielectric permittivity of the corundum component is by about two orders-of-magnitude smaller than the dielectric permittivity of the FC (see Table 1 and experimental results [10–15]). It should be added that, to the best of our

Table 1 Room temperature elastic moduli c_{ab}^E (in 10¹⁰ Pa), piezoelectric coefficients e_{ij} (in C/m²) and dielectric permittivities $\epsilon_{pp}^\xi/\epsilon_0$ of poled ZTS-19 FC and corundum ceramic

Constants	ZTS-19 FC [3]	Corundum ceramic [11, 12]
c_{11}^E	10.9	43.6
c_{12}^E	6.1	12.3
c_{13}^E	5.4	12.3
c_{33}^E	9.3	43.6
c_{44}^E	2.4	15.7
e_{31}	−4.9	0
e_{33}	14.9	0
e_{15}	10.6	0
$\epsilon_{11}^\xi/\epsilon_0$	820	10
$\epsilon_{33}^\xi/\epsilon_0$	840	10

ZTS is the abbreviation used to term Pb(Zr, Ti)O₃-based FC compositions Elastic moduli of corundum ceramic (isotropic medium) were evaluated by taking into account experimental values of Young’s modulus $Y = 382$ GPa [11] and Poisson’s ratio $\nu = 0.22$ [12]. These values are consistent with experimental constants $Y = 403$ GPa and $\nu = 0.2353$ measured at temperature $T = 296$ K [13]

knowledge, the performance of a piezo-active 3–0-type composite containing a stiff inorganic component and FC has yet to be studied in detail by taking into account the specific composite microgeometry and elastic properties of the components. Most probably, a difference between the elastic properties of the piezoelectric and piezo-passive components (see Table 1) has the potential to strongly influence the piezoelectric properties and electromechanical coupling of composites in specific volume-fraction ranges. In the present paper, we describe new experimental results on elastic properties and piezoelectric resonance-antiresonance frequencies in a corundum-containing 3–0-type composite and interpret these results by taking into consideration model concepts and composite structure-property relations.

2 Manufacturing of composite samples

Samples of the piezo-active corundum-containing composite were manufactured at ‘Piezopribor’, Institute of High Technologies and Piezotechnics, Southern Federal University. The only piezoelectric component of this composite is the ZTS-19 FC based on Pb(Zr, Ti)O₃, and the electromechanical properties of the ZTS-19 FC in the poled state (Table 1) are similar to the electromechanical properties of some PZT-type FCs [2, 4]. The corundum ceramic (94.39% mass fraction of Al₂O₃ therein) is piezo-passive and characterised by a high elastic stiffness (see Table 1). Corundum ceramic samples were first pressed and sintered by means of the conventional ceramic technology [7, 15]. After cooling, the sintered samples were crushed under pressure to obtain corundum ceramic particles with an average size from a specific range. The corundum particles and ZTS-19 FC powder were carefully mixed, and the mass fraction $f_{m,c}$ of the corundum component was chosen from the range of 2.5 mass % $\leq f_{m,c} \leq 10.0$ mass %.

Pressed disk-shaped samples were sintered in a lead-containing medium at the heating rate 50 K/h, temperature 1513 K, and time range 2 h. The cooling process was relatively long, without an appointed rate of cooling. The composite samples were disk-shaped, with a diameter $d_s = 10.00 \pm 0.06$ mm and height $h_s = 1.00 \pm 0.07$ mm.

3 Experimental results on contents, microgeometry, and parameters of the composite

Shrinkage of the manufactured composite samples Δ^* in the sintering stage was studied to evaluate the effective density ρ^* of the composite and volume fractions of components therein. A link between the corundum mass fraction $f_{m,c}$ (in mass %) and Δ^* (in %) is expressed in the polynomial form as follows:

$\Delta^*(f_{m,c}) = 9.91 - 1.17f_{m,c} + 0.0238f_{m,c}^2$. The above given formula suggests that $\Delta^*(f_{m,c})$ decreases on increasing the mass fraction (and therefore, the volume fraction) of the corundum component.

Relations between the corundum mass fraction $f_{m,c}$ and volume fractions of the corundum ceramic m_c and air pores m_p in the non-poled composite samples are shown in Table 2 for four values of $f_{m,c}$. We observe the ‘mirror’ behaviour of the volume fractions m_c and m_p , and this behaviour has no analogies among the piezo-active 3–0-type composites studied earlier.¹ In our opinion, such an original behaviour of m_c and m_p is achieved due to specifics of the shrinkage Δ^* of the composite samples wherein the high stiffness corundum component influences the internal mechanical stress field and pore formation, especially for relatively small m_c values. We remind the reader that the relatively large difference in the elastic moduli of the corundum and FC components (Table 1) is one of the main features of the studied composite, and the pore formation can be regarded as a specific stress accommodation in the composite sample due to the mismatch of the elastic properties of the FC and corundum components.

Examples of micrographs of sections of the non-poled composite samples (Fig. 1a–c) suggest that the composite microgeometry becomes more complicated on increasing the corundum mass fraction $f_{m,c}$. We observe a coexistence of the corundum-rich regions (inclusions) and air pores and an increase in the porosity m_p of the composite on increasing $f_{m,c}$. The average size of the pores increases on increasing $f_{m,c}$ (cf., for instance, Fig. 1c, b), and this leads to a higher stress relief in the composite sample. The systems of the pores and corundum inclusions become more intensively spread over the composite sample on increasing $f_{m,c}$ (cf. Fig. 2a, c). For reference, in Fig. 1d, we show a microstructure of the non-poled dense FC wherein the porosity level is small in comparison to the composite in Fig. 1a–c. The difference between the micrographs in Fig. 1a, b is less pronounced than the difference between the micrographs in Fig. 1b, c. In our opinion, this is related to features of the aforementioned $\Delta^*(f_{m,c})$ dependence and, therefore, with conditions for the formation of pores in the studied $f_{m,c}$ range.

Based on the micrographs from Fig. 1a–c and other experimental results, we note that the studied composite can be characterised as that belonging to the 3–0-type composites, where 3 is related to the FC component, and 0 is related to the corundum component. The connectivity formula for the

¹ It should be mentioned for comparison that, according to experimental results [10] on the corundum-containing composite, the relative porosity of the sample increases quickly, as the volume fraction of $\alpha\text{-Al}_2\text{O}_3$ increases from 0 to 0.10, and on increasing the volume fraction of $\alpha\text{-Al}_2\text{O}_3$ from 0.10 to 0.60, the relative porosity increases almost linearly. Authors [10] explain such a behaviour of the relative porosity by the existence of non-shrinking $\alpha\text{-Al}_2\text{O}_3$ phase that restricts shrinkage of the ceramic matrix during sintering.

Table 2 Experimental data on the mass fraction $f_{m,c}$ of corundum ceramic and volume fractions of corundum m_c and air m_p in composite samples

$f_{m,c}$ (mass %)	m_c	m_p
2.5	0.052	0.086
5.0	0.097	0.117
7.5	0.135	0.151
10	0.170	0.174

studied composite can be written as 3–0–0, where the extra 0 on the right position is related to the isolated air pores that are seen in Fig. 1.

The composite samples were poled in air at the electric field $E = 1.25$ kV/mm and temperature $T = 638$ K, and the total poling time was 75 s. The effective electromechanical properties and related parameters were measured on the composite samples after a week. These measurements were performed by means of the resonance-antiresonance method [14, 15], and frequencies were measured to an accuracy of 3%. The poled composite is characterised by ∞ mm symmetry, and the remanent polarisation of the composite is $\mathbf{P}_r^* \parallel OX_3$ in the rectangular co-ordinate system ($X_1X_2X_3$). In the present paper, we analyse the following parameters of the poled disk-shaped composite samples:

- piezoelectric resonance frequencies f_r and f_{rt} at the planar and thickness oscillation modes, respectively,
- piezoelectric antiresonance frequencies f_a and f_{at} at the planar and thickness oscillation modes, respectively, and
- elastic compliance s_{11}^{*E} at electric field $E = \text{const}$, elastic modulus c_{33}^{*D} at electric displacement $D = \text{const}$, and Poisson’s ratio $\nu^{*E} = -s_{12}^{*E}/s_{11}^{*E}$ at $E = \text{const}$.

A relation between the resonance frequency f_r at the planar oscillation mode of the disk-shaped composite sample ($h_s \ll d_s$) and its elastic properties [14] is given by

$$s_{11}^{*E} = F(\nu^{*E})(\rho^*)^{-1}(\pi d_s f_r)^{-2}, \quad (1)$$

and the main resonance frequency range $[f_r, f_a]$ is concerned with the ratio

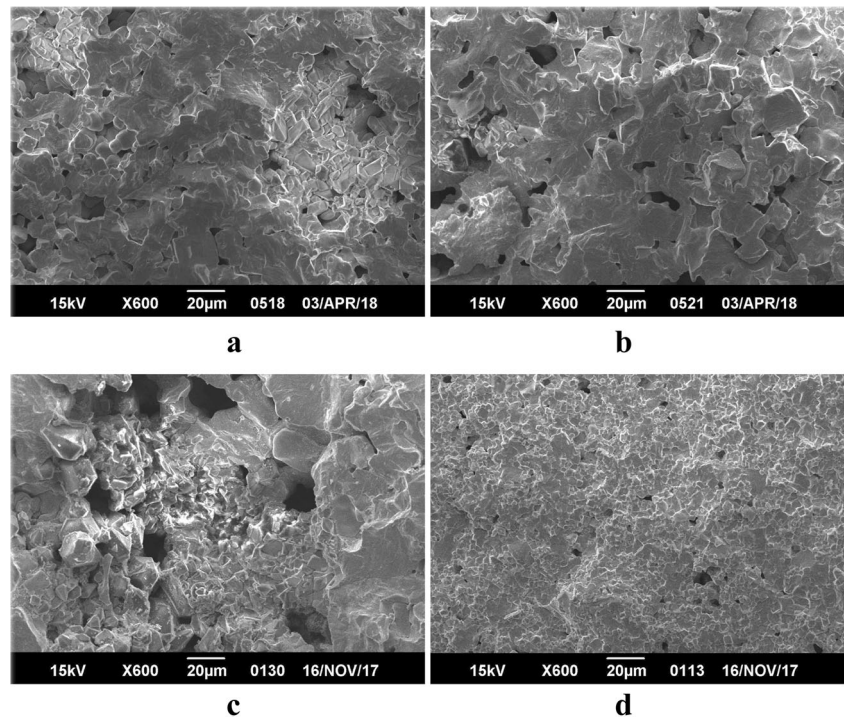
$$\delta_p = (f_a - f_r)/f_r. \quad (2)$$

In Eq. (1), $F(\nu^{*E}) = [0.4(\nu^{*E})^2 + 2.4\nu^{*E} + 3.4] / [1 - (\nu^{*E})^2]$, and $\pi = 3.14159\dots$ The absolute value of the planar electromechanical coupling factor (ECF) k_p^* is linked to δ_p from Eq. (2) as follows:

$$|k_p^*| = ((a/\delta_p) + b)^{-1/2}. \quad (3)$$

The ECF is used [14, 15] to characterise a piezoelectric material on effectiveness of a conversion of energy from the mechanical form into the electric form and vice versa. Based

Fig. 1 Micrographs of sections of the ZTS-19 FC/corundum/air composite manufactured at the mass fraction of corundum $f_{m,c} = 2.5\%$ (a), 5.0% (b), and 7.5% (c). Micrograph (d) is related to the dense ZTS-19 FC, i.e. $f_{m,c} = 0$. Micrographs were taken using JEOL JSM-6390L Analytical Electron Microscope



on our experimental results, we represent a and b from Eq. (3) as polynomials $a = 0.418 - 0.0724\nu^{*E} - 0.00366(\nu^{*E})^2$ and $b = 0.619 - 0.163\nu^{*E} + 0.0403(\nu^{*E})^2$. We mention that values of $a = 0.399$ and $b = 0.581$ [15] are also used to evaluate k_p^* from Eq. (3) for the disk-shaped piezoelectric element at its planar oscillation mode.

At the thickness oscillation mode, the antiresonance frequency f_{at} is linked [14, 15] to the elastic modulus c_{33}^{*D} of the composite in accordance with the relation

$$c_{33}^{*D} = \rho^* (2h_s f_{at})^2. \tag{4}$$

The main resonance frequency range $[f_r, f_{at}]$ is found from the formula

$$\delta_t = (f_{at} - f_{rt}) / f_{rt}, \tag{5}$$

and δ_t from Eq. (5) is linked [15] to the thickness ECF k_t^* in accordance with the formula

$$k_t^* = ((0.405/\delta_t) + 0.810)^{-1/2}. \tag{6}$$

Experimental results shown in Fig. 2 suggest that the studied composite for relatively small volume fractions of corundum ($m_c < 0.18$) is characterised by the following performance. The ECF anisotropy $k_t^* / |k_p^*|$ (cf. curves 1 and 2 in Fig. 2a) becomes more pronounced on increasing m_c and at minor changes of k_t^* and ν^{*E} (see curves 2 and 3 in Fig. 2a). The effective density ρ^* decreases due to the corundum

component and air pores. The elastic properties of the composite demonstrate either minor changes (s_{11}^{*E} , see curve 5 in Fig. 2a) or appreciable changes (c_{33}^{*D} , see curve 6 in Fig. 2a). This means that the corundum component and porosity influences the elastic response of the composite along the poling direction OX_3 to a large extent. The appreciable decrease of $|k_p^*|$ at $k_t^* \approx \text{const}$ (see curves 1 and 2 in Fig. 2a) can be related to a weakening of the electromechanical coupling along the non-polar direction (OX_1) on increasing m_c , and this corresponds to the larger porosity level of the composite. Examination of micrographs in Fig. 1 suggests that the system of the corundum inclusions and air pores can lead to the considerable weakening of the electromechanical coupling along the non-polar direction. This weakening is expected to be more appreciable in a case of Fig. 1c which is related to the larger mass fraction of corundum $f_{m,c}$, volume fraction of corundum m_c , and porosity of the sample m_p . We remind the reader that the average pore size in Fig. 1c is larger than the average pore size in Fig. 1a, b, and this also weakens the transverse piezoelectric response and electromechanical coupling concerned with k_p^* .

Based on our data on the resonance (antiresonance) frequencies in Fig. 2b, we state $f_r \approx \text{const}$ and slow decreasing f_a (cf. curves 1 and 2 in Fig. 2b) at the planar oscillation mode. The frequencies f_{rt} and f_{at} at the thickness oscillation mode decrease on increasing m_c (see curves 3 and 4 in Fig. 2b). The steady character of the $f_r(m_c)$ dependence is accounted for by conditions $F(\nu^{*E}) \approx \text{const}$ and $s_{11}^{*E} \rho^* \approx \text{const}$ which are valid in the studied m_c range.

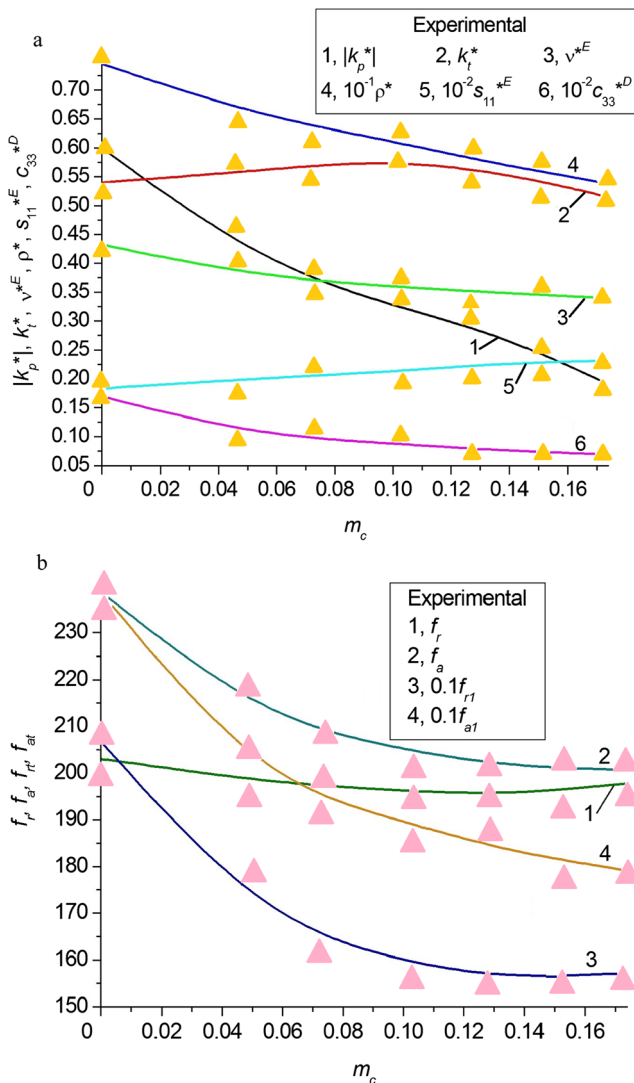


Fig. 2 Experimental data on ECFs k_p^* and k_t^* ((a) curves 1 and 2), Poisson’s ratio ν^{*E} ((a) curve 3), density ρ^* (in kg/m^3 , (a) curve 4), elastic compliance s_{11}^{*E} (in 10^{-12} Pa^{-1} , (a) curve 5), elastic modulus c_{33}^{*D} (in 10^{10} Pa , (a) curve 6), resonance frequencies f_r and f_{rt} (in kHz, (b) curves 1 and 3), and antiresonance frequencies f_a and f_{at} (in kHz, (b) curves 2 and 4) of the ZTS-19 FC/corundum/air composite samples at room temperature

The f_a and δ_p from Eq. (2) are linked to k_p^* from Eq. (3), and therefore, one can surmise a definite influence of the electromechanical coupling along OX_1 on f_a .

For the thickness oscillation mode, the antiresonance frequency f_{at} (see curve 4 in Fig. 2b) decreases due to a decrease of the c_{33}^{*D}/ρ^* ratio on increasing m_c . Comparing curves 4 and 6 in Fig. 2a, we see that c_{33}^{*D} decreases more intensively than ρ^* , and this leads to the decreasing $f_{at}(m_c)$ dependence in accordance with Eq. (4). It should be noted that the frequency range $[f_{rt}, f_{at}]$ remains almost constant (see curves 3 and 4 in Fig. 2b), and such a feature is concerned with $k_t^* \approx \text{const}$ and $\delta_t \approx \text{const}$ [see curve 2 in Fig. 2a and Eqs. (5) and (6)].

4 Modelling analysis

Our interpretation of the elastic properties and resonance frequencies from Eqs. (1), (2), (4), and (5) is carried out for the disk-shaped piezo-active composite sample (Fig. 3a) at $d_s \gg h_s$. Hereby, we put forward the ‘composite in composite’ model (Fig. 3b). The main elements of this model are composite rods surrounded by a porous FC matrix. A system of corundum inclusions is regularly distributed in a poled FC matrix, and such a distribution leads to the 3–0 connectivity pattern (see inset 1 in Fig. 3b). The FC/corundum rods are parallel to the poling axis OX_3 and surrounded by the porous 3–0 matrix (see inset 2 in Fig. 3b). The shape of each corundum inclusion obeys the equation

$$(x_1/a_1)^2 + (x_2/a_2)^2 + (x_3/a_3)^2 = 1. \tag{7}$$

In Eq. (7), $a_1, a_2 = a_1$, and a_3 are semi-axes of the spheroidal inclusion, and $\rho_c = a_1 / a_3$ is its aspect ratio. The spheroidal shape of the air pore with the semi-axes $a_1', a_2' = a_1'$, and a_3' and the aspect ratio $\rho_p = a_1'/a_3'$ is described by the equation that is similar to Eq. (7). It is assumed that the air pores are also regularly distributed in the FC medium. Because of the presence of corundum and air in the rods and matrix, respectively (Fig. 3b), the volume fraction of the corundum component in the composite is $m\mu_c$, and porosity of the composite is $(1 - m)\mu_p$.

The effective electromechanical properties of the 3–0-type composite (Fig. 3b) are determined as follows. In the first stage, the effective electromechanical properties of the 3–0 FC / corundum and 3–0 FC / air composites are evaluated by using the method [16, 17] and Eshelby’s concept on spheroidal inclusions in heterogeneous solids [18]. The effective properties of the 3–0 porous FC medium at the dilute approximation [16] are expressed in the matrix form as follows:

$$\|C^{(pm)}\| = \|C^{(FC)}\| \cdot \left[\|I\| - \mu_p \left(\|I\| - (1 - \mu_p) \|S_p\| \right)^{-1} \right]. \tag{8}$$

The dilute approximation [16] means that no interaction between the isolated air pores is considered in the porous medium. In Eq. (8),

$$\|C^{(FC)}\| = \left(\begin{array}{c} \|c^{(FC),E}\| \|e^{(FC)}\|^t \\ \|e^{(FC)}\| - \|e^{(FC),\xi}\| \end{array} \right) \tag{9}$$

is the 9×9 matrix of the electromechanical properties of FC, $\|I\|$ is the 9×9 identity matrix, $\|S_p\|$ is the 9×9 matrix that comprises components of the electroelastic Eshelby tensor from work [18]. Elements of $\|S_p\|$ depend [16] on the aspect

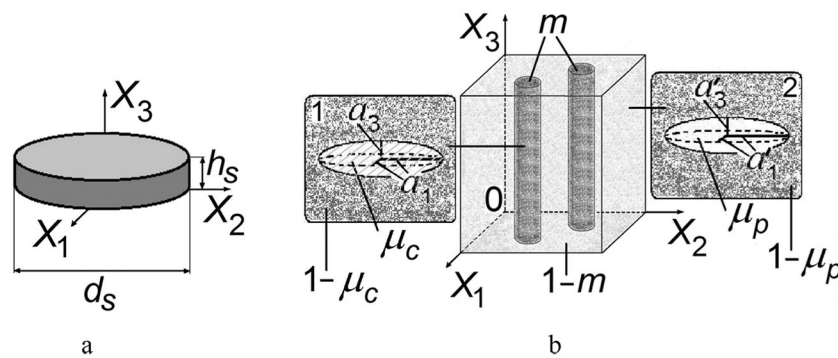


Fig. 3 Schematic of the disk-shaped composite sample **(a)** and 3–0-type composite **(b)**. $X_1X_2X_3$ is a rectangular co-ordinate system. In **a**, d_s is the diameter of the sample, and h_s is the height (thickness) of the sample. In **b**, m and $1 - m$ are the volume fractions of the rods and surrounding matrix, respectively. In the inset 1 of **b**, μ_c is the volume fraction of the corundum

inclusions in the FC medium, $1 - \mu_c$ is the volume fraction of the FC medium, and a_1 and a_3 are semi-axes of the corundum inclusion. In the inset 2 of **b**, μ_p is the porosity, $1 - \mu_p$ is the volume fraction of the FC medium surrounding the air pores, and a_1' and a_3' are the semi-axes of the air pore

ratio ρ_p of the pore and on the properties of the FC medium. In Eq. (9), $\|c^{(FC),E}\|$ is the 6×6 matrix of elastic moduli at electric field $E = \text{const}$, $\|e^{(FC)}\|$ is the 3×6 matrix of piezoelectric coefficients, $\|\varepsilon^{(FC),\xi}\|$ is the 3×3 matrix of dielectric permittivities at mechanical strain $\xi = \text{const}$, and superscript ‘ t ’ denotes the transposition.

The effective properties of the 3–0 FC/corundum rod at the dilute approximation [3, 16] are expressed in the matrix form as

$$\|C^{(r)}\| = \|C^{(FC)}\| + \mu_c \left(\|C^{(c)}\| - \|C^{(FC)}\| \right) \quad (10)$$

$$\left[\|I\| + \|S_c\| \|C^{(FC)}\|^{-1} \left(\|C^{(c)}\| - \|C^{(FC)}\| \right) \right]^{-1}.$$

In Eq. (10), $\|C^{(c)}\|$ and $\|C^{(FC)}\|$ characterise the properties of corundum and FC, respectively, and have the structure shown in Eq. (9). Elements of $\|S_c\|$ from Eq. (10) depend on the aspect ratio ρ_c of the corundum inclusion and on the properties of the FC medium that surrounds it (see inset 1 in Fig. 3b).

In the second stage, the effective properties of the 3–0-type composite (Fig. 3b) are found for the system of the poled 3–0 FC/corundum cylindrical rods in the 3–0 FC/air matrix. This matrix can be either poled (i.e piezo-active) or non-poled (i.e piezo-passive), and the poling axis is OX_3 . In fact, the rods/matrix system represents the 1–3-type composite for which the effective field method [3, 17, 18] is applicable. Following this method, we take into account the electromechanical interactions in the composite system (Fig. 3b) and find the effective electromechanical properties of the studied composite from the formula

$$\|C^*\| = \|C^{(pm)}\| + m \left(\|C^{(r)}\| - \|C^{(pm)}\| \right) \left[\|I\| + (1-m) \|S\| \|C^{(pm)}\|^{-1} \left(\|C^{(r)}\| - \|C^{(pm)}\| \right) \right]^{-1} \quad (11)$$

In Eq. (11), $\|C^{(pm)}\|$ and $\|C^{(r)}\|$ are taken from Eqs. (8) and (10), respectively. Elements of $\|S\|$ from Eq. (11) are related

to the circular cylinder (see the rod shape in inset 1 in Fig. 3b) and depend on the aspect ratio ρ_c of the corundum inclusion and on the properties of the surrounding FC medium (see inset 1 in Fig. 3b). The matrix (11) can be represented as $\|C^*\| = \|C^*(m, \rho_c, \rho_p, \mu_c, \mu_p)\|$, and its structure is similar to that shown in Eq. (9). Based on elements of $\|C^*\|$ from Eq. (11) and formulae [12, 15, 19] for the piezoelectric medium and taking Eqs. (1), (2), (4), (5) into account, we evaluate the elastic compliances s_{ab}^{*E} , elastic moduli c_{fg}^{*E} and c_{fg}^{*D} , ECFs k_i^* and k_p^* , resonance and antiresonance frequencies, etc.

As follows from our analysis of the effective properties from Eq. (11), ECFs k_i^* and k_p^* , and other parameters of the composite, the oblate corundum inclusions can effectively influence the anisotropy of ECFs and piezoelectric and elastic properties of the composite. In Fig. 4, we show examples of the volume-fraction (m_c) dependence of the parameters evaluated for the composite with the heavily oblate corundum inclusions ($\rho_c = 100$). Hereby, the porous matrix that surrounds the corundum/FC rods can be either poled (at $\rho_p = 1$, see graphs in Fig. 4a–c, e) or non-poled (at $\rho_p = 100$, see graph in Fig. 4d). A better agreement between the evaluated and experimental parameters of the composite is achieved in the presence of the poled porous matrix; however, the m_c range where this agreement is observed (Fig. 4a–c, e) is not very wide. The resonance and antiresonance frequencies f_r and f_a , respectively (Fig. 4a, b), depend on μ_c and μ_p . Such a behaviour may be concerned with an idealisation in the composite model (Fig. 3b), for instance, with assumptions on the regular distribution of the corundum inclusions and air pores in the FC medium, on the constant aspect ratios ρ_c and ρ_p , on the ideal rod shape of regions where the corundum inclusions are distributed, etc.

For the antiresonance frequency f_{at} at the thickness oscillation mode, agreement between the calculated and experimental results is achieved for the composite with the poled rods and matrix at $m_c \approx 0.06$ – 0.17 (Fig. 4c). When replacing the poled

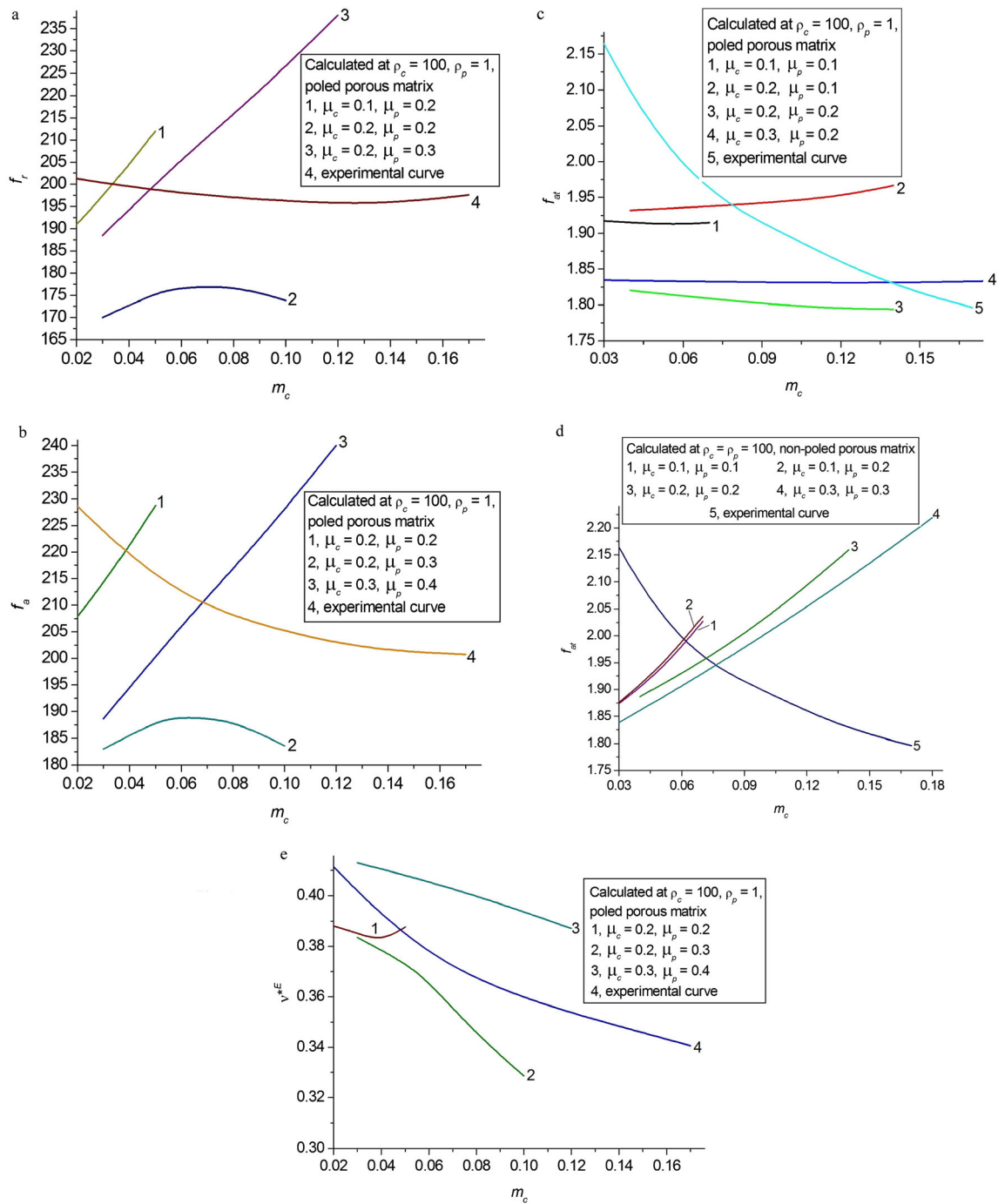


Fig. 4 Volume-fraction (m_c) dependences of the resonance frequency f_r (in kHz, **a**) and antiresonance frequency f_a (in kHz, **b**) at the planar oscillation mode, antiresonance frequency f_{at} (in MHz, **c**, **d**) at the thickness oscillation mode, and Poisson's ratio ν^{*E} (**e**) which are

calculated for the ZTS-19 FC/corundum/air composite sample at $d_s = 10.00$ mm and $h_s = 1.00$ mm (see the schematic in Fig. 3a). Calculations were performed by using experimental data from Table 1. Experimental curves of the studied parameters are given for comparison

matrix with the non-poled matrix at $\rho_p = 100$, we observe a restricted agreement between the calculated and experimental results in a narrower volume-fraction range, at $m_c \approx 0.06$ – 0.10 (Fig. 4d). This means that the poling degree and shape of the pore in the matrix can strongly influence the elastic properties and frequency characteristics of the composite. In accordance

with Eq. (4), the antiresonance frequency f_{at} depends on the elastic modulus c_{33}^{*D} . The c_{33}^{*D} is concerned with the elastic action and response along the poling axis OX_3 and depends on the aspect ratios ρ_c , ρ_p , volume fractions m , m_c , and m_p , specifics of porous structures in the matrix, etc. Our evaluations of the resonance frequency f_{rt} at the thickness oscillation mode

suggest that the equality $f_{at} - f_{rt} \approx 300$ kHz is valid at $m_c \leq 0.17$, and this is consistent with experimental data (see curves 3 and 4 in Fig. 2b). Finally, as follows from Fig. 4e, the $\nu^{*E}(m_c)$ dependence can be explained within the framework of the composite model (Fig. 3b) at $m_c \approx 0.03$ – 0.12 .

It is also important to compare values of the frequency constant N_t that depends on the resonance frequency f_{rt} at the thickness oscillation mode in accordance with the formula [14, 15] $N_t = f_{rt} h_s$, where h_s is the height (thickness) of the disk-shaped sample (see Fig. 3a). Based on our experimental data (see curve 3 in Fig. 2b) at $h_s = 1.00$ mm, we have $N_t \approx 1.6$ – 2.0 kHz m in the volume-fraction range of $m_c \approx 0.05$ – 0.17 . The aforementioned N_t values are comparable to those related to the conventional monolithic PZT-4, PZT-5 [14], PZT-5A, PZT-5H, and PZT-8 FCs [20]. The frequency constant $N_p = f_r d_s$ at the planar oscillation mode, $d_s = 10.00$ mm, and $f_r \approx 0.2$ MHz for the studied composite (see curve 1 in Fig. 2b) equals ca. 2 kHz m. For the monolithic PZT-4, PZT-5A, PZT-5H, and PZT-8 FCs, experimental values of N_p are in the range of 1.93 kHz m $\leq N_p \leq 2.34$ kHz m [20], i.e. no considerable deviations from N_p of the composite are observed. However, the studied composite is characterised by the larger anisotropy of ECFs k_t^*/k_p^* in comparison to the conventional PZT-type FCs [14, 15, 20], and this performance and other characteristics of the composite are to be taken into consideration when selecting piezoelectric materials for transducers, sensors, electroacoustic devices, etc.

5 Conclusions

In the present paper, we have manufactured and studied the 3–0-type FC/corundum ceramic/air composite wherein the PZT-type FC is the only piezoelectric component in the poled state. In general, this composite can be characterised as a modern piezoelectric material with relatively stable resonance (f_r and f_{rt}) and antiresonance (f_a and f_{at}) frequencies at volume fractions of the corundum ceramic $0.05 < m_c < 0.18$. The corundum ceramic, being a component with high Young's modulus compared to the FC matrix, influences the elastic properties, anisotropy of ECFs k_t^*/k_p^* , porosity, and other parameters of the composite. As seen from experimental curves in Fig. 2, this influence can be strong [e. g. $k_p^*(m_c)$, $\rho^*(m_c)$, and $s_{11}^{*E}(m_c)$], moderate [e. g. $c_{33}^{*D}(m_c)$, $f_a(m_c)$, $f_{rt}(m_c)$, and $f_{at}(m_c)$], or weak [e. g. $k_t^*(m_c)$, $\nu^{*E}(m_c)$ and $f_r(m_c)$].

The volume-fraction (m_c) behaviour of the elastic properties and piezoelectric resonance (antiresonance) frequencies (Fig. 2) is interpreted in terms of the 'composite in composite' model (Fig. 3b) where the 3–0 connectivity patterns are used to describe the distribution of the corundum inclusions and air pores over the sample. Despite the definite idealisation in the

present model, it can be applied to interpret the elastic properties and frequency characteristics of the 3–0-type composite. The presence of the corundum and air components at their volume fractions $m_c \approx m_p$ (see Table 2) influences the electro-mechanical properties of the composite and can promote the observed stability of the resonance (antiresonance) frequencies. The heavily oblate corundum inclusion and the poled porous FC matrix in the model put forward enable us to reach agreement between the calculated and experimental results (see Fig. 4a–c, e) at various sets of input parameters of the model (μ_c , μ_p , ρ_c , and ρ_p). Due to the performance (Fig. 2) analysed in the present paper, the 3–0-type corundum-containing composite can be used as an active element of piezoelectric transducers, acoustic, and other devices wherein the thickness oscillation mode plays the important role.

Acknowledgements The authors would like to thank Prof. Dr. A. A. Nesterov and Prof. Dr. I. A. Parinov (Southern Federal University, Rostov-on-Don, Russia) and Prof. Dr. C. R. Bowen (University of Bath, UK) for their continuing interest in the performance of modern piezoelectric materials. Special thanks are extended to Prof. Dr. C. R. Bowen for his careful reading of the manuscript and valuable comments.

Funding information Research has been carried out at the financial support from the Ministry of Education and Science of the Russian Federation within the framework of the complex project "Working out and creation of a high-technological production of a mobile hydroacoustic complex to highlight a situation in various areas of the World ocean on the basis of modern piezoelectric means of the new generation" (contract No. 03.G25.31.0276, May 29th, 2017) by using the equipment of the Centre of Collective Use "High Technologies" at the Southern Federal University.

Compliance with ethical standards

Conflict of interest The authors declare that they have no conflict of interest.

References

1. Safari A, Akdogan EK (2006) Rapid prototyping of novel piezoelectric composites. *Ferroelectrics* 331:153–179. <https://doi.org/10.1080/00150190600737727>
2. Smay JE, Tuttle B, Cesarano J III (2008) Robocasting of three-dimensional piezoelectric structures. In: Safari A, Akdoğan EK (eds) *Piezoelectric and acoustic materials for transducer applications*. Springer, New York, pp 305–318. <http://www.springer.com/la/book/9780387765389>
3. Topolov VY, Bowen CR (2009) *Electromechanical properties in composites based on ferroelectrics*. Springer, London. <http://www.springer.com/gp/book/9781848009998>
4. Akdogan EK, Allahverdi M, Safari A (2005) Piezoelectric composites for sensor and actuator applications. *IEEE Trans Ultrason Ferroelec Freq Contr* 52:746–775 <http://ieeexplore.ieee.org/document/1503962/>
5. Newnham RE, Skinner DP, Cross LE (1978) Connectivity and piezoelectric-pyroelectric composites. *Mater Res Bull* 13:525–536. [https://doi.org/10.1016/0025-5408\(78\)90161-7](https://doi.org/10.1016/0025-5408(78)90161-7)

6. Chaipanich A (2007) Dielectric and piezoelectric properties of PZT–cement composites. *Curr Appl Phys* 7:537–539. <https://doi.org/10.1016/j.cap.2006.10.015>
7. Filippov SE, Vorontsov AA, Topolov VY, Brill OE, Bisegna P, Panich AE (2014) Features of the piezoelectric effect in a novel PZT-type ceramic/clay composite. *Ferroelectrics Lett Sec* 41:82–88. <https://doi.org/10.1080/07315171.2014.950101>
8. Dongyu X, Xin C, Shifeng H (2015) Investigation of inorganic fillers on properties of 2–2 connectivity cement/polymer based piezoelectric composites. *Constr Build Mater* 94:678–683. <https://doi.org/10.1016/j.conbuildmat.2015.07.090>
9. Zhao P, Kim S, Hinderliter B (2016) Investigation of cement–sand-based piezoelectric composites. *J Intel Mater Syst Struct* 27:1666–1672. <https://doi.org/10.1177/1045389X15600901>
10. Rybyanets AN, Konstantinov GM, Naumenko AA, Shvetsova NA, Makar'ev DI, Lugovaya MA (2015) Elastic, dielectric, and piezoelectric properties of ceramic lead zirconate titanate/ α -Al₂O₃ composites. *Phys Solid State* 57:527–530 <https://link.springer.com/content/pdf/10.1134/S1063783415030270.pdf>
11. Grigoryev IS, Meylikhov EZ (eds) (1991) Physical values: reference book. Energoatomizdat, Moscow (in Russian)
12. MatWeb: material property data. www.matweb.com
13. Goto T, Anderson OL (1989) Elastic constants of corundum up to 1825 K. *J Geophys Res* 94:7588–7602. <https://doi.org/10.1029/JB094iB06p07588>
14. Berlincourt DA, Cerran DR, Jaffe H (1964) Piezoelectric and piezomagnetic materials and their function in transducers. In: W. Mason (ed.) *Physical acoustics. Principles and methods*. V.1. Methods and devices. Pt A. New York: Academic, p. 169–270. <https://www.elsevier.com/books/physical-acoustics/mason/978-1-4832-2857-0>
15. Ruschmeyer K, Helke G, Koch J, Lubitz K, Möckl T, Petersen A, Riedel M, Schönecker A (1995) *Piezokeramik: Grundlagen, Werkstoffe, Applikationen*. Renningen-Malmsheim: Expert
16. Dunn ML, Taya M (1993) Electromechanical properties of porous piezoelectric ceramics. *J Am Ceram Soc* 76:1697–1706. <https://doi.org/10.1111/j.1151-2916.1993.tb06637.x/abstract>
17. Dunn M (1993) Micromechanics of coupled electroelastic composites: effective thermal expansion and pyroelectric coefficients. *J Appl Phys* 73:5131–5140. <https://doi.org/10.1063/1.353787>
18. Huang JH, Yu S (1994) Electroelastic Eshelby tensors for an ellipsoidal piezoelectric inclusion. *Compos Eng* 4:1169–1182. [https://doi.org/10.1016/0961-9526\(95\)91290-W](https://doi.org/10.1016/0961-9526(95)91290-W)
19. Ikeda T (1990) *Fundamentals of piezoelectricity*. Oxford University Press, Oxford
20. Sherman CH, Butler JL (2007) *Transducers and arrays for underwater sound*. Springer, New York. <http://www.springer.com/us/book/9781441921987>